

# Boreal summer quasi-monthly oscillation in the global tropics

Bin Wang · Peter Webster · Kazuyoshi Kikuchi ·  
Tetsuzo Yasunari · Yanjun Qi

Received: 16 September 2005 / Accepted: 22 May 2006 / Published online: 3 August 2006  
© Springer-Verlag 2006

**Abstract** The boreal summer intraseasonal oscillation (ISO) in the global tropics is documented here using a 7-year suite (1998–2004) of satellite measurements. A composite scenario was made of 28 selected events with reference to the oscillation in the *eastern* equatorial Indian Ocean (EIO), where the oscillation is most regular and its intensity is indicative of the strength of the subsequent northward propagation. The average oscillation period is about 32 days, and this quasi-monthly oscillation (QMO) is primarily confined to the tropical Indian and Pacific Oceans. Topics that were investigated are the partition of convective versus stratiform clouds, the vertical structure of precipitation rates, and the evolution of cloud types during the initial organization and the development of intraseasonal convective anomalies in the central Indian Ocean.

During the initiation of the convective anomalies, the stratiform and convective rains have comparable rates; the prevailing cloud type experiences a *trimodal evolution* from shallow to deep convection, and finally to anvil and extended stratiform clouds. A major northwest/southeast-slanted rainband forms as the equatorial rainfall anomalies reach Sumatra, and the rainband subsequently propagates *northeastward* into the west Pacific Ocean. The enhanced precipitation in the west Pacific then rapidly traverses the Pacific along the Intertropical Convergence Zone, meanwhile migrating northward to the Philippine Sea. A *seesaw teleconnection* in rainfall anomalies is found between the southern Bay of Bengal (5–15°N, 80–100°E) and the eastern Pacific (5–15°N, 85–105°W). Local sea-surface temperature (SST)-rainfall anomalies display a negative simultaneous correlation in the off-equatorial regions but a zero correlation (quadrature phase relationship) near the equator. We propose that atmosphere–ocean interaction and the vertical monsoon easterly shear are important contributors to the northeastward propagation component of the intraseasonal rainband. The observed evidence presented here provides critical information for validating the numerical models, and it supports the self-induction mechanism theory for maintenance of the boreal summer ISO.

---

B. Wang (✉) · K. Kikuchi  
Department of Meteorology and the International Pacific  
Research Center (IPRC), University of Hawaii,  
1680 East West Road, POST Bldg. 409E,  
Honolulu, HI 96822, USA  
e-mail: wangbin@hawaii.edu

P. Webster  
School of Earth & Atmospheric Science  
& Civil and Environmental Engineering,  
Georgia Tech University, Atlanta, GA, USA

T. Yasunari  
Hydrospheric and Atmospheric Research Center,  
Nagoya University, Nagoya, Japan

Y. Qi  
Laboratory of Numerical Modeling for Atmospheric  
Sciences and Geophysical Fluid Dynamics (LASG),  
Institute of Atmospheric Physics,  
Chinese Academy of Science, Beijing, China

## 1 Introduction

During the boreal summer, the equatorial-trapped, eastward-propagating Madden and Julian (1971, 1972) Oscillation (MJO) weakens considerably; major centers of intraseasonal variability in precipitation and

low-level zonal winds shift to monsoon trough regions in the Northern Hemisphere (Lau and Chan 1988; Wang and Rui 1990; Salby and Hendon 1994; Kemball-Cook and Wang 2001, among others). Northward propagation prevails in the northern Indian Ocean (e.g., Yasunari 1979, 1980; Sikka and Gadgil 1980; Krishnamurti and Subrahmanyam 1982; Webster 1983; Goswami and Shukla 1984), while the intraseasonal variability in the western North Pacific features salient westward and northwestward propagation (e.g., Murakami 1980; Lau and Chan 1986; Chen and Murakami 1988). The complex behavior of boreal summer intraseasonal oscillation (ISO) has previously been documented by using the following datasets: reanalysis products from the National Centers for Environmental Prediction-National Center for Atmospheric Research (NCEP-NCAR) and the European Centre for Medium-Range Weather Forecasts (ECMWF), outgoing longwave radiation (OLR), rawinsonde, and results from the atmospheric general circulation model (GCM) (Hartmann et al. 1992; Ferranti et al. 1997; Webster et al. 1998; Krishnan et al. 2000; Anamalai and Slingo 2001; Kemball-Cook and Wang 2001; Hsu and Weng 2001; Lawrence and Webster 2002).

The lack of accurate observations over the tropical oceans has been a major impediment in detecting the oscillation's initiation and evolution processes. Even using the same data (e.g., OLR), ambiguous results have been produced by studies that use different statistical methods. For instance, the composite study of Kemball-Cook and Wang (2001) found that the initial negative OLR anomalies starts from the western equatorial Indian Ocean (EIO); however, the composite life cycle, based on an MJO index derived from a multivariate empirical orthogonal function (EOF) analysis, showed that the OLR anomalies start from the eastern EIO (Wheeler and Hendon 2004). And, the regression analysis of Jiang and Li (2005) suggested the OLR anomalies originating from the western coast of Equatorial Africa, whereas Lawrence and Webster (2002) found that some ISOs form in the western EIO while others form in the eastern EIO.

Using data from the Tropical Rainfall Measuring Mission (TRMM), Wang et al. (2005)—hereafter referred to as WWT05—found that the antecedents of the active and break periods of the monsoon emerge in the western EIO, and the initiation of a new rainy phase is preceded by in situ surface wind convergence and central EIO warming. Unfortunately, these conclusions were derived based on only 3 years of data, and the focus of WWT05 was on the Indian monsoon

only. The present study uses 7 years of TRMM data and the study's scope extends beyond the Indian monsoon region. In this study, we were especially interested in a global picture of the boreal summer ISO and the intraseasonal linkage between the Indian and Pacific Oceans.

Knowledge of the vertical structure of heating distribution and the cloud's evolution during the initial organization and development of intraseasonal convective anomalies is critical for validating our ISO simulations of GCMs; this knowledge is vital because the uncertainties in mathematical descriptions of these interactive parameterizations could jeopardize the model's capability to simulate the ISO. Johnson et al. (1999) found that MJO involves trimodal (deep, congestus, shallow) distribution of convection in the western Pacific (see also Kikuchi and Takayabu 2004). Increased vertical resolution of the numerical model undoubtedly more accurately resolves the melting layer and cumulus congestus, thus providing a more realistic simulation of the MJO (Slingo et al. 2003). Unfortunately, little is known about the vertical-distribution precipitation and evolution of clouds in the ISO generation over the Indian Ocean. Use of TRMM precipitation radar (PR) data to examine cloud evolution during reinitiation of the boreal summer ISO is a unique aspect of the present study.

Section 2 explains data and analysis methods used in this study. Next is a satellite perspective of the mean life cycle in terms of (1) the ISO rainfall (Sect. 3) and (2) the sea-surface temperature (SST) anomalies (Sect. 4). Section 5 documents an intraseasonal seesaw teleconnection between the Indian and the eastern Pacific monsoons. In Sect. 6, variations in the vertical profiles of precipitation and cloud types during the initiation process are presented. Section 7 discusses the mechanisms for monsoon ISO, drawing upon the results derived from the present analyses and previous studies. The final section summarizes our research and findings and discusses remaining issues.

## 2 Data and analysis method

The TRMM data provide an unprecedented opportunity for the investigation of the ISO evolution and structure over those oceanic regions that have been typically devoid of traditional data. The semi-equatorial orbit of the TRMM satellite allows data be collected at various local times in any given Earth location between 35°S and 35°N (Kummerow et al. 1998). This yields an improved estimate of daily mean

precipitation rate as well as atmospheric water vapor and liquid cloud water. The TRMM microwave imager (TMI) can measure a number of variables in the presence of clouds, including SST, precipitable water, and precipitation (Wentz and Spencer 1998; Chelton et al. 2001). The TMI data used in this study is produced by Remote Sensing Systems and sponsored by the NASA Earth Science REASoN DISCOVER Project and can be found at <http://www.remss.com>. The resolution of the original data was  $0.25 \times 0.25$  degrees of latitude/longitude from which we made  $2^\circ \times 2^\circ$  averaged data for the present study. Since TMI rainfall data are available only over the ocean, the precipitation datasets TRMM 3B42 and PR2a25 have also been used. The 3B42 precipitation data blend microwave measurements, visible and infrared measurements, and adjust precipitation estimates based on the Geostationary Operational Environmental Satellite (GOES) precipitation index, yielding precipitation estimates over both ocean and land areas with a resolution of  $2 \times 2$  degrees of latitude/longitude. The PR2a25 products are estimated from the TRMM precipitation radar, which provides three-dimensional rain-rate profiles for each cell (measuring  $4 \text{ km} \times 4 \text{ km} \times 250 \text{ m}$ ) and information about the stratiform and convective rains.

The surface winds and convergence are derived from the QuikSCAT scatterometer (National Aeronautics and Space Administration 2001). The data were downloaded from the website of the Air–Sea Interaction & Climate Team, which is a group in the Jet Propulsion Laboratory in Pasadena, California. The GCM ECMWF reanalysis product ER40 is used only to complement the satellite data. The reanalysis data was downloaded from the following web site: <http://www.ecmwf.int/products/data/archive/descriptions/e4/>.

To extract signals of intraseasonal variability, a Lanczos band-pass filter was applied to the daily data (Duchon 1979). A composite method similar to WWT05 was used to document the mean behavior of the ISO. Special attention was paid to two important issues for making an adequate composite: the selection of the reference time series and the determination of the composite time interval. We chose a reference time series of precipitation averaged in the eastern EIO ( $5^\circ\text{S}$ – $5^\circ\text{N}$ ,  $75$ – $100^\circ\text{E}$ ). This is essentially the same region chosen by Lawrence and Webster (2002) and also by WWT05. This location sees the largest intraseasonal variability of rainfall in the tropics, yet most atmospheric GCMs have difficulty reproducing the observed intraseasonal variability (Waliser et al. 2003). As ISOs tend to form either in the western and central EIO or in situ in the eastern EIO, this reference location

would seem ideal. The intraseasonal variation of the precipitation in this region is nearly  $180^\circ$  out of phase with that over the central India and the northern Bay of Bengal. Therefore, this reference location might also be representative of the active/break cycles of the South Asian monsoon. And, as the boreal summer ISO expands into the Pacific Ocean, our choice of base reference will facilitate the detection of subsequent behavior in the Pacific.

A time series of daily precipitation rates averaged over the reference region is shown in Fig. 1a. The 20–50 day oscillation component is predominant and generally accounts for 60–70% of the total square root variance in the time series. Thus, the 20–50 day band-pass-filtered component is used to produce composite scenarios. From 1998 through 2004, each summer experienced several active break periods between mid-May and mid-September, providing a total of 28 cycles with significant magnitude (a rain rate greater than  $5 \text{ mm/day}$ ) for the peak positive phase and the two adjacent negative phases. These 28 events were selected for inclusion in constructing a composite; each event is indicated by a double-sided arrow in Fig. 1a.

Nearly all of these strong cycles are associated with a well-organized northward propagation from the equator to the South Asian region (Fig. 1b). Figure 1b shows that the northward propagation is more systematic from May to August and is less well defined during September and October. The ISOs that were not chosen generally have relatively small amplitudes and also tend to correspond to ill-organized northward propagations, suggesting that the ISO strength in the eastern EIO is an indication of the intensity of broad-scale northward propagation.

The periods of individual cycles are notably irregular. We defined the oscillation period of an individual event as the time interval around a selected peak, spanning from the preceding minimum to the ensuing minimum. The periods of 26 out of the 28 individual cycles range from 24 to 40 days (Fig. 1a). The average period for the 28 cycles is about 32 days per cycle; thus, the mean interval between two adjacent phases is about 4 days. The boreal summer ISO has a shorter period than the boreal winter MJO.

Since the periods are irregular, the method used to construct the composite life cycle was based on eight consecutive phases in each of the 28 cycles. Phases 1, 3, 5, and 7 correspond to, respectively, the times when rainfall anomalies are at a minimum, a positive transition (negative-turning-to-positive) phase, a maximum, and a negative transition phase. Thus, Phases 1 and 5 represent the driest and the wettest phases, respectively, in the eastern EIO. This phase-dependent

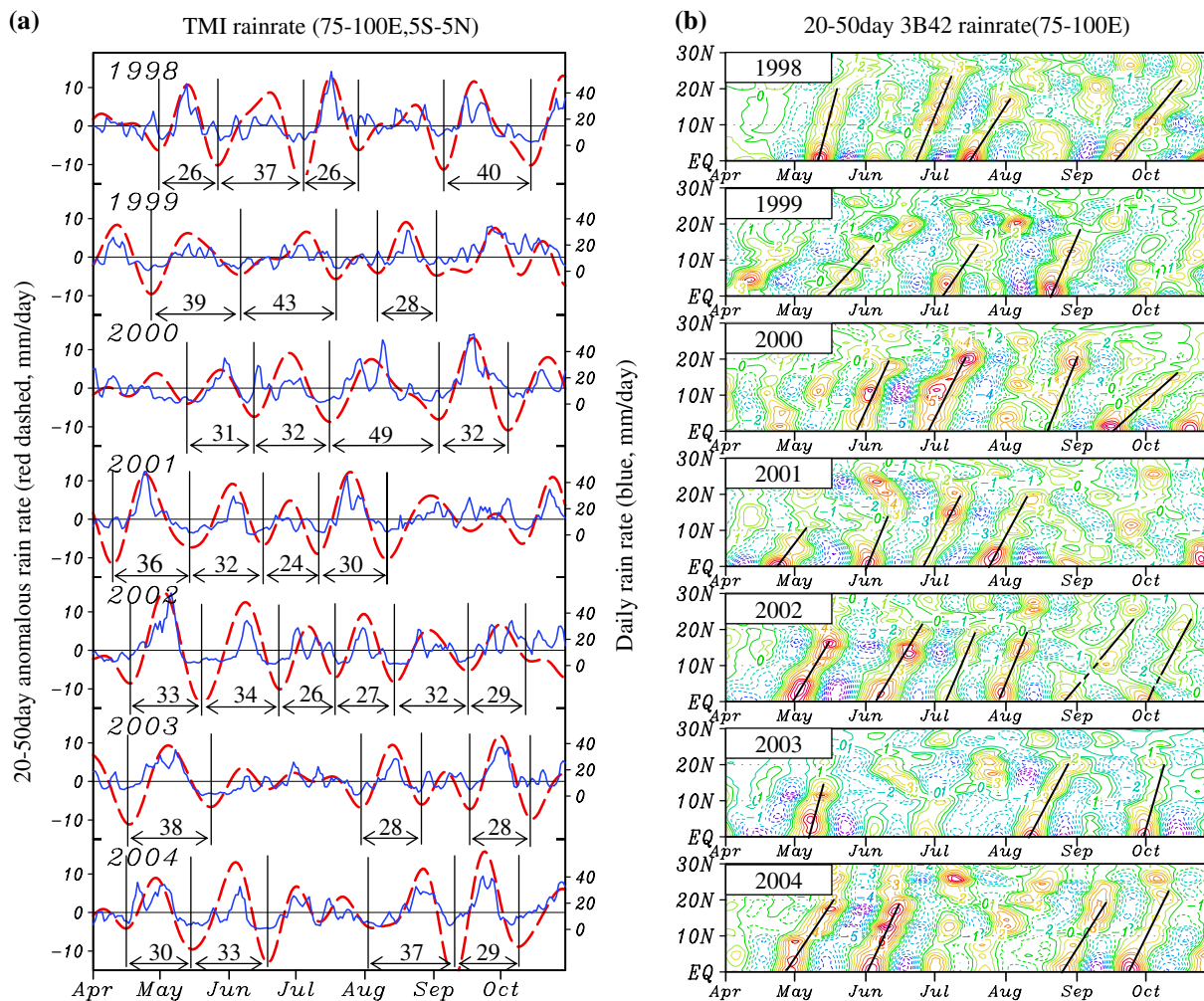


**Fig. 1** a TRMM/TMI precipitation rate averaged over the eastern EIO (5°S–5°N, 75–100°E). Blue represents the 3-day running mean, and red shows the 20–50 day anomalies; double-headed arrows indicate the selected 28 events, along with time

period in days; b time-latitude plot of the 20 to 50-day filtered TMI 3B42 daily precipitation rate (mm/day<sup>-1</sup>) averaged between 75 and 100°E. The slanted lines indicate the northward propagation of the ISO's rainy phase

composite has advantages over regression analysis with respect to the reference time series at different fixed lags (days) and also has advantages over other analyses in which the period is considered as fixed. In the latter methods, when individual oscillation periods are highly irregular, the derived composite evolution would mix up different phases of the oscillation cycles, which is undesirable when detecting transition ISO phases (re-initiation or generation).

Statistical analysis was applied to the composite fields. Based on the Student *t*-test, the findings showed that statistical significant at the 90% confidence level for (1) the magnitude of anomalous rainfall rate is greater than 2 mm day<sup>-1</sup> and (2) the magnitude of anomalous SST is greater than 0.1°C (refer to the composite maps in Fig. 2).

### 3 A satellite perspective of the boreal summer QMO rainfall anomalies

Figure 2 presents a composite eight-phase QMO life cycle of the TMI precipitation rate and SST anomalies in the global tropics. The figure shows only the Indian and Pacific sector (2/3 of the tropics) because the TMI precipitation and SST anomalies over the Atlantic sector are insignificant, suggesting that the global QMO is primarily confined to the tropical Indo-Pacific domain. Major features of positive rainfall anomalies are highlighted using black solid lines; negative anomalies are indicated with dashed lines. For convenience, the following description will focus on the positive (wet) anomalies, but the formation and propagation of dry anomalies follow a similar footprint as

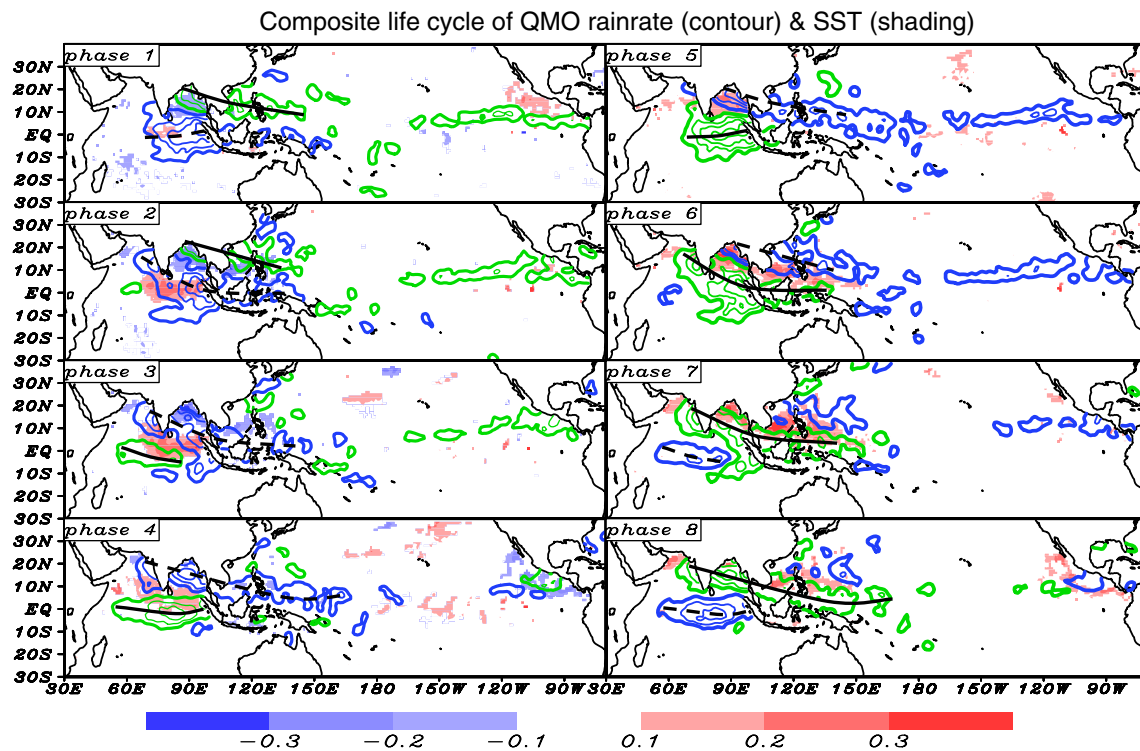


**Fig. 2** Composite eight-phase life cycle of the boreal summer QMO. Green denotes positive precipitation rate (TRMM/TMI) anomalies starting from  $2 \text{ mm day}^{-1}$  with contour intervals of  $3 \text{ mm day}^{-1}$ ; lavender shows negative anomalies starting from  $-2 \text{ mm day}^{-1}$ . The major features of positive rainfall anomalies

are highlighted using *black solid lines*; *dashed lines* indicate negative anomalies. Shading represents sea-surface temperature (SST) anomalies in units of degrees Celsius. Only statistically significant rainfall and SST anomalies at 90% confidence level are shown

the enhanced rainfall anomalies across the Indo-Pacific during the complete QMO cycle.

Phase 1 features a minimum rainfall in the eastern EIO and a peak wet monsoon over the head Bay of Bengal. About 4 days later (Phase 2), a small area of organized positive rainfall anomalies first emerges in the western EIO between  $60$  and  $70^\circ\text{E}$ , initiating the next spell of QMO rainfall. In Phase 3, the new rainfall-anomaly area expands eastward along  $5^\circ\text{S}$  and further develops into a heavy precipitation region that becomes symmetric about the equator in Phase 4. Phases 1 through 3 can be viewed as the genesis process for a new wet phase of the QMO cycle.

Rainfall anomaly in the eastern EIO reaches a peak during Phase 5; meanwhile, rainfall has ceased over India. Note that at this stage, anomalous convection over Sumatra weakens considerably. Meanwhile, the anomalously wet region bifurcates poleward, transforming into a V-shaped rainband that tails the main center of the equatorial convection; this is Phase 6 of the life cycle. The V-shaped rainband is highly asymmetric about the equator and is far stronger in the Northern Hemisphere (NH). Thus, the major rainband displays a northwest/southeast-tilted structure in the

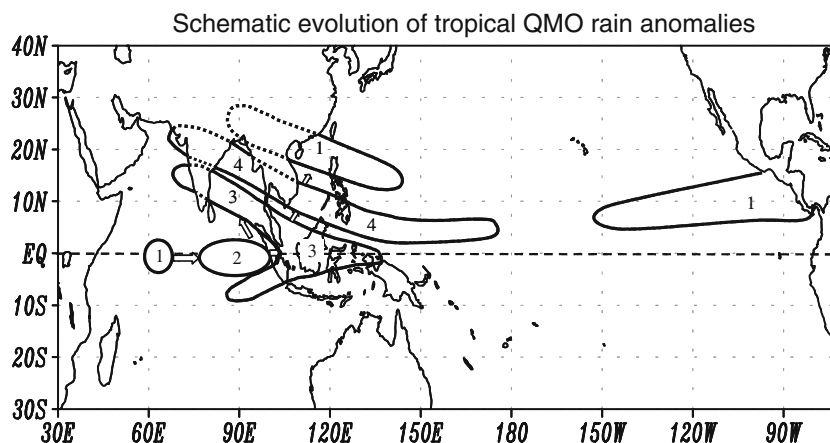
NH, extending from the Arabian Sea to the equatorial western Pacific (Phases 6 and 7), concurrent with suppressed convection restarting in the western EIO.

The life cycle continues with the northward and eastward propagation of the enhanced rainband in the northern Indian and western Pacific Oceans, from Phase 6 to the Phase 1 of the next cycle, causing a peak activity period in the Indian monsoon. Although the strongest fluctuations associated with the QMO are in the Indian Ocean and the western North Pacific, coherent signals are seen to swiftly traverse the North Pacific along the Intertropical Convergence Zone (ITCZ) from Phase 8 to the next Phase 1.

The results derived by using 3B42 product are extremely consistent with the results derived from the TMI data (figure not shown). The major difference between the 3B42 and TMI data lies in their amplitudes. The amplitude of precipitation derived from TMI tends to be twice larger than that of 3B42 for some reasons (e.g., Kummerow et al. 2000).

Figure 3 highlights the life cycle shown in Fig. 2. The evolutionary cycles of wet and dry QMO anomalies follow similar paths. The evolution of wet phase includes (1) the initiation of rainfall anomalies in the

**Fig. 3** Schematic diagram showing four stages of the boreal summer QMO wet and dry anomalies: (1) initiation, (2) maturity, (3) formation of the slanted precipitation band, and (4) northeastward propagation. Each stage lasts about 8 days



EIO from 60 to 70°E and their subsequent development and eastward propagation along the equator; (2) the formation of a slanted band of rainfall anomalies, tilted from the maritime continent to India; (3) the *northeastward* migration of the rainband in the northern Indian and western North Pacific Oceans, and (4) the rapid spread of these rainfall anomalies along the ITCZ to the eastern North Pacific (ENP) and concurrent slow northward migration to the Philippine Sea.

#### 4 SST anomalies in association with the intraseasonal rainfall anomalies

A striking feature seen in Fig. 2 is that significant SST anomalies occur in a systematic manner throughout the QMO life cycle. For instance, from Phase 3 to 7, warm SST anomalies are always located northeast of the convective anomalies; i.e., the rainfall anomaly tends to move toward the area of ocean surface warming. The implication of this phase relationship will be further discussed in Sect. 7.

Due to lack of daily observation of precipitation over the oceans, the SST-precipitation relationship associated with boreal summer ISO have been studied by using OLR (e.g., Kemball-Cook and Wang 2001; Stephens et al. 2004) or MSU data (e.g. Fasullo and Webster 2000; Webster et al. 2002) as a proxy to precipitation. The SST data that were used are from NCEP reanalysis (weekly resolution interpreted to daily). These studies found that intraseasonal SST anomalies tend to be in quadrature with intraseasonal convective anomalies (e.g., Fasullo and Webster 2000; Kemball-Cook and Wang 2001; Webster et al. 2002; Stephens et al. 2004). At odds with others, Vecchi and Harrison (2002) found a lag of the same length but opposite in sign, with cold water leading precipitation. Here, we used the best available satellite observations

and further scrutinize the intraseasonal SST-rainfall relationship.

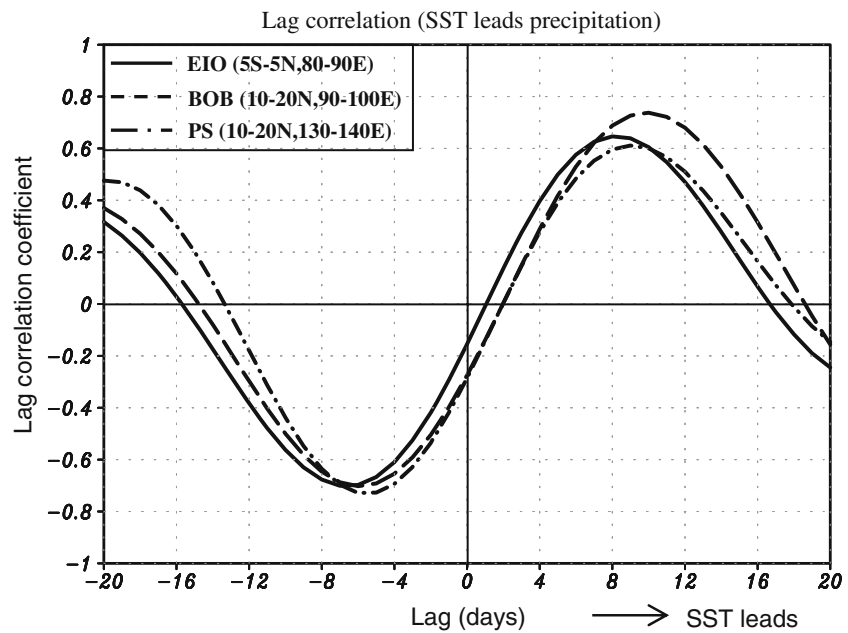
To see the phase relationship between local SST and rainfall anomalies, we show, in Fig. 4, their lag correlation coefficients computed for three regions of the largest ISO variability: the eastern EIO, the head Bay of Bengal, and the Philippine Sea. A positive time lag means that SST leads rainfall. Over the eastern EIO, the SST and rainfall anomalies exhibit a nearly perfect quadrature temporal phase relationship, thus the simultaneous correlation coefficient is nearly zero. However, this is not true in the off-equatorial monsoon regions, i.e., the Bay of Bengal and the Philippine Sea. In these areas, the ocean surface warming tends to lead enhanced convection by about 10 days, but the enhanced rainfall leads ocean surface cooling by about 5 days. Of note is that the simultaneous correlation between SST and rainfall anomalies is not zero but a significant negative value (between  $-0.2$  and  $-0.3$ ). What is new here is that the SST-precipitation relation is different between the equatorial and off-equatorial regions.

The intraseasonal SST-rainfall relationship can be realistically reproduced using the coupled atmosphere-ocean model for boreal winter eastward propagation of MJO (Waliser et al. 1999) and northward-propagating monsoon ISO (Fu et al. 2003), but not in the AGCM-alone simulations in which the SST and rainfall anomalies tend to be in phase (Wu et al. 2002; Fu and Wang 2004). This suggests that the observed SST-Precipitation relationship results from atmosphere-ocean interaction.

#### 5 Intraseasonal seesaw between the Indian and ENP monsoons

Figure 2 shows that the rainfall anomalies over the southern Bay of Bengal (5–15°N, 80–100°E) tend to be

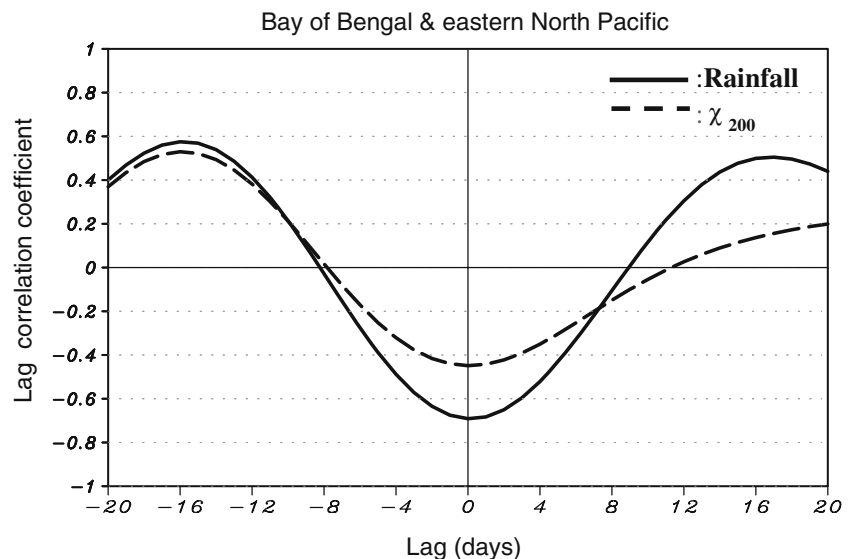
**Fig. 4** Lag correlation coefficients between SST and precipitation (TRMM/3B42) QMO anomalies at three key locations. A positive lag indicates that SST leads precipitation. The computation periods are from May 1 to September 30 over the central equatorial Indian Ocean (EIO) (5°S–5°N, 80–90°E) and the Bay of Bengal (10–20°N, 90–100°E), and from June 1 to October 31 over the Philippine Sea (10–20°N, 130–140°E). The sample size at each location is 900



out of phase with anomalous rainfall over the ENP (5–15°N, 85–105°W), a region that has typical monsoon features (Murakami et al. 1992). Figure 5 shows the lag correlation between QMO rainfall anomalies in the two regions, which confirms the seesaw feature shown in Fig. 2. The maximum correlation coefficient is about –0.60 for a sample size of 900 occurring at lag –16 day, implying that the rainfall anomaly in the southern Bay of Bengal leads the anomaly in the ENP by about 16 days. Meanwhile the minimum concurrent negative correlation is about –0.70, implying that it is out of phase by nearly 180°. A stronger negative correlation pattern exists in the 200 hPa-velocity potential field (Fig. 5).

WWT05 has shown that during the re-initiation of new convective anomalies, the EIO is under control of large-scale upper-level convergence and subsidence; when deep convection starts in the central EIO, a negative OLR anomaly develops locally, and upper-level divergence occurs later as a *result* of deep convection rather than because of it (Fig. 4, WWT05). Using 7-year data, we constructed a composite evolution of 200 hPa-velocity potential anomalies derived from ECMWF reanalysis along with TRMM 3B42 rainfall anomalies. The derived figure is similar to Fig. 4 in WWT05 and is therefore not shown here. However, we want to add two remarks to WWT05.

**Fig. 5** Lag correlation coefficients in QMO rainfall anomalies from TRMM/3B42 (solid line) and the 200 hPa-velocity potential anomalies (dashed line) between the southern Bay of Bengal (5–15°N, 80–100°E) and the eastern North Pacific (ENP, 5–15°N, 85–105°W). The negative lag indicates that the Bay of Bengal leads ENP



First, different to the MJO, the upper-level velocity potential throughout the entire QMO cycle shows a marked stationary wavenumber one pattern with two opposite polarities located at 90°E and 90°W, respectively. The simultaneous negative correlation between the southern Bay of Bengal (90°E) and the ENP (90°W), shown in Fig. 5, reflects this stationary wavenumber-one feature and suggests a stationary pulsation of anomalous Walker circulation on the quasi-monthly time scale, which is consistent with the negative correlation in the rainfall anomalies between the southern Bay of Bengal and the ENP. Second, during the persistence of the stationary seesaw pattern, the 200 hPa-velocity potential perturbation over the Indian Ocean experiences a northward propagation from Phases 1 to 3 (and Phases 5 to 7) and a transformation from a monopole structure to a north-south dipole pattern in the Indian Ocean. From Phases 3 to 4, the upper-level divergence wave shows a rapid eastward movement across the Pacific and Atlantic Oceans, leading to an opposite phase of the seesaw pattern. This reversal of the anomalous Walker circulation is driven by the rapid development of the strong convection over the eastern EIO and the arrival of dry anomalies in the ENP after the dry anomalies rapidly traverse the Pacific.

## 6 Changes in the rainfall profile and cloud properties during the genesis process

Figure 6 shows rain rate profile anomalies during Phases 1 through 3 in the region of initiation (5°S–5°N, 60–70°E). The anomalies are defined as deviations from the eight-phase mean profile. The rain rate profile below 1 km was not shown in order to avoid complications arising from signal clutter. During Phase 1, there is a slightly positive anomaly increasing downward below 4 km in total rainfall rate, which is almost solely attributed to convective rain (Fig. 6a). Both convective and stratiform types of rain develop rapidly from Phases 1 to 2. During Phase 2, the amount of convective rain is about 1.5 times that of stratiform rain (Fig. 6b). The vertical distributions of rainfall rate for both types show typical properties that are similar to those in the previous study using TRMM PR data (Liu and Fu 2001) and that have been explained by previous investigators (e.g., Houze 1993, Chap. 6). From Phases 2 to 3, the total rainfall rate changes little, but the ratio between convective and stratiform rain decreases markedly (Fig. 6c). At this stage, the amount of stratiform rain is about 1.5 times that of convective rain.

The above results suggest the following sequence of cloud development during the genesis process of QMO. In Phase 1, shallow convection develops first, followed by rapidly deepening convective development in Phase 2. Finally, in Phase 3, stratiform clouds predominate. This hypothesis is consistent with some previous studies (Kemball-Cook and Weare 2001; Wu 2003) that focused on different locations (the Maritime Continent and the western Pacific Ocean, respectively) and during different seasons (primarily, the boreal winter). More importantly, the stratiform precipitation has a rate comparable to that of convective clouds, which may provide a rigorous test for GCMs.

## 7 Discussion: mechanisms of boreal summer QMO

### 7.1 How is the QMO sustained?

Explanations of the initiation and maintenance of the boreal summer ISO have been contentious. WWT05 discussed this issue, and our current discussion here draws upon that research. Rodwell (1997) proposed that a dry phase (break) in the summer South Asian monsoon could be triggered by the injection of high negative-potential vorticity air coming from Southern Hemisphere extratropical disturbances and entering a low-level monsoon flow. However, the extratropical weather systems of both hemispheres are essentially chaotic, with time scales spanning days. In the absence of some selection criteria, it is difficult to attribute the relatively regular low-frequency variations of the QMO to mid-latitude weather noise. Model studies by Wang and Xie (1997) suggested that the off-equatorial Rossby waves could transfer energy to the equatorial region through basic-state Hadley circulation and could then invigorate equatorial convective anomalies. However, the means of transfer were not addressed. Krishnan et al. (2000) speculated that decoupling of the eastward-propagating equatorial anomaly and the northwestward-propagating descending Rossby waves from the central Bay of Bengal might contribute to the transition from a wet phase to a break phase in the Indian summer monsoon. But, the reasons for why decoupling occurs and how decoupling generates new convective anomalies were left as unanswered questions.

Stephens et al. (2004) suggested that the hydrological cycle associated with the ISO acts as a self-regulating oscillator. They argued that regulation occurs as a feedback between radiation processes and hydrological processes in the atmosphere. It is argued that

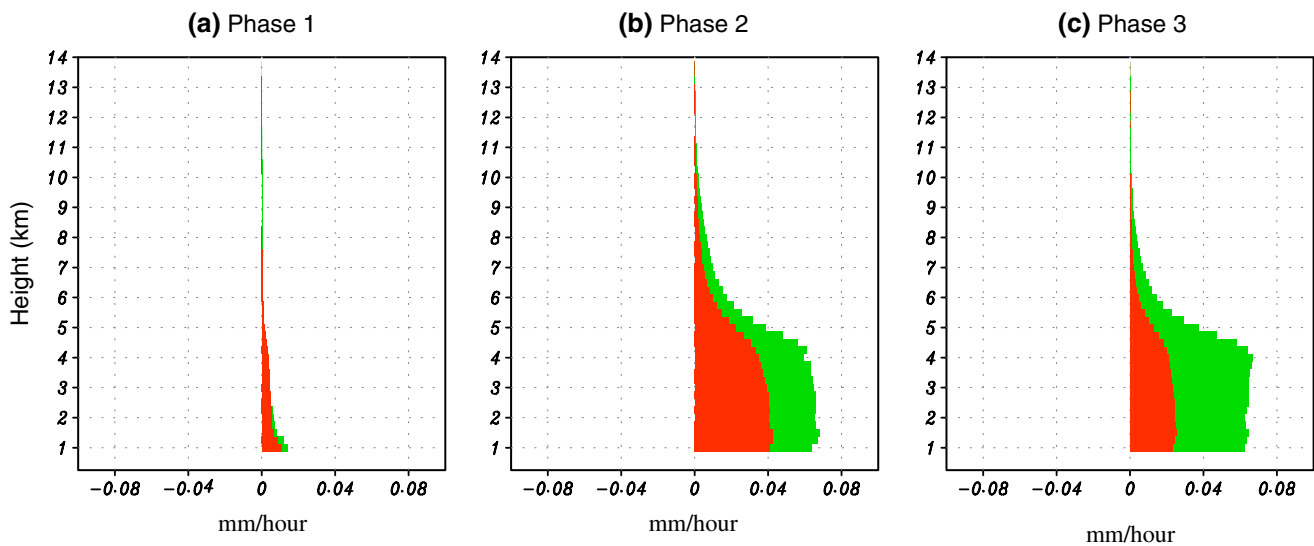


**Fig. 6** Composite vertical profiles of precipitation rate anomalies associated with QMO measured by the TRMM precipitation radar (TRMM/2A25) over the EIO ( $5^{\circ}\text{S}$ – $5^{\circ}\text{N}$ ,  $60$ – $70^{\circ}\text{E}$ ) where

ISO initiates. Each phase spends about 4 days. *Red* and *green* color represent convective and stratiform rain rate, respectively

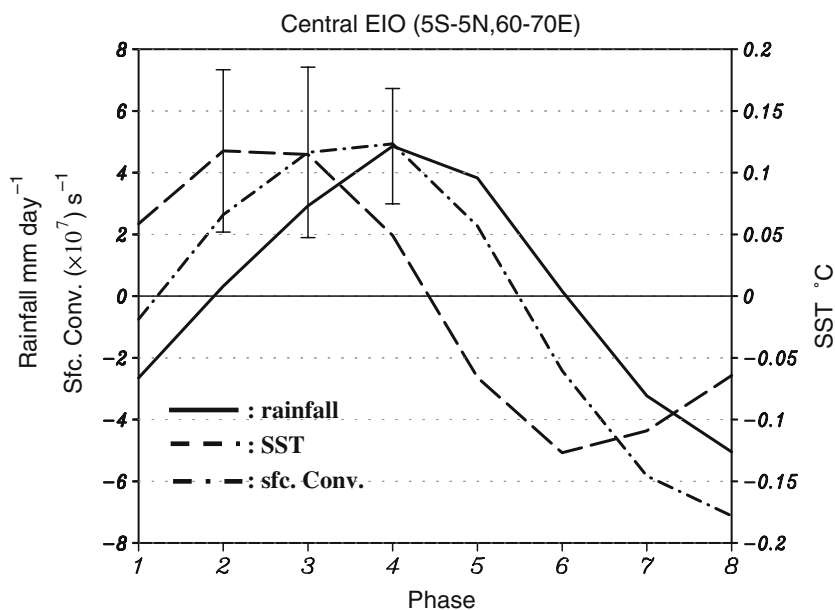
there are three main phases to self-regulating oscillation: (1) a destabilization phase in which the surface layer of the ocean heats while the upper atmosphere radiatively cools, (2) a convective phase in which deep convection grows in the heated ocean region as available potential convective energy is released, and (3) a restoring and stabilizing phase in which SST is cooled by strong winds and reduced radiation, while the upper atmosphere is radiatively heated, leading to a reduction of convection and a calming of the winds. Stephens et al. (2004) noted the importance of the hydrological cycle in explaining time scales spanning 30–60 days as a natural oscillator through feedbacks between local thermodynamics and dynamic responses. Note that their argument does not take into account the complex feedback of atmospheric circulation that occurs in both space and time. Stephens et al. (2004) also argued that the heating of the ocean during the undisturbed phase is a necessary condition.

The dashed line in Fig. 7 shows the composite life cycle of the SST and the rainfall anomalies in the QMO initiation region ( $5^{\circ}\text{S}$ – $5^{\circ}\text{N}$ ,  $60$ – $70^{\circ}\text{E}$ ). The warming leads rainfall anomalies by about 1.5 phase, which suggests that sea-surface warming may precondition the initiation. On the other hand, although weak positive SST anomalies appear over the EIO in Phase 1 before the occurrence of the new rainfall anomaly (Fig. 2), the occurrence of the new convective anomalies (Phase 2) does not take place directly above the maximum SST anomalies, suggesting that the in situ weak SST warming is not sufficient in the initiation of new convective anomalies.

Complementary to the argument made by Stephens et al. (2004), WWT05 took into consideration the role of dynamics of the atmospheric circulation. Using 3 years of data (1999–2001), WWT05 showed that the local moisture convergence in the western-central EIO occurs in Phase 1 before the re-initiation of the next QMO cycle. To confirm this finding, we show in Fig. 7 the composite life cycle of the surface convergence in the initiation region where QuikSCAT data give reliable estimations (dot-and-dash line in Fig. 7). The surface convergence leads rainfall anomalies by about one half to one phase, suggesting that the surface convergence may play a critical role in initiating the new ISO convection. WWT05 proposed that both the in situ surface wind convergence and the central EIO warming are induced by the anomalous conditions set up in the previous cycle; therefore, a self-induction mechanism is acting in maintaining the Indian monsoon active-break cycle. The present study supports this hypothesis through the use of an extended dataset and further suggests that this self-induction mechanism plays a key role in maintaining the global scale boreal summer QMO.

Why does this self-induction mechanism occur only in the western-central Indian Ocean? The main reason is that the strongest QMO convective anomalies during the boreal summer is located in the eastern EIO, which creates the strongest surface divergence/convergence to its west through atmospheric Rossby wave response and creates SST anomalies to its west when it moves eastward and encounters the blocking of the Sumatra Island. WWT05 showed that the upper-level

**Fig. 7** Composite life cycle of rainfall (TRMM/TMI), surface convergence, and SST anomalies in the initiation region (5°S–5°N, 60–70°E). The bar segments represent 90% confidence interval based on the Student *t*-test



divergence wave does not lead the development of the new convection over the central EIO; rather it is a result of the Indian Ocean ISO convective development. Once the ISO strongly developed in the Indian Ocean sector, the upper-level circulation anomalies eventually propagate eastward. The region outside of the Indian Ocean sector is thus a passive response to the strong oscillation in the northern Indian Ocean. That is why the EIO is a key region for the recurrence of the QMO. The ocean surface warming and surface convergence that are critical for generation of a new wet ISO cycle is essentially a result of the dry phase in the eastern EIO in the previous cycle. The specific phase-locking development of boreal summer QMO determines the Indian Ocean is conducive for self-induction.

## 7.2 Why does the QMO rainband move northeastward?

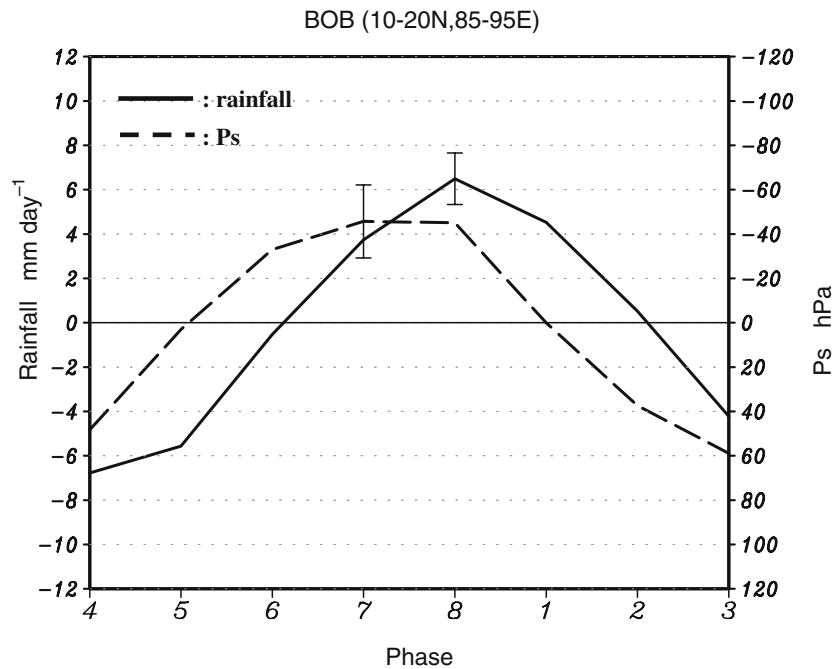
The present results show that the northward propagation over the eastern Indian Ocean (Fig. 1b) is a two-dimensional manifestation of the northeastward movement of the slanted rainband (Fig. 2). The two-dimensional northward propagation of QMO has stimulated numerous studies in the last two decades, producing a large number of hypotheses and theories (for a detailed review, see Wang 2005). Here, we argue that air–sea interaction may be one of the contributing factors in the northeastward propagation of the intra-seasonal rainband.

How can air–sea interaction enhance northeastward propagation? As shown in Sect. 4, the air–sea interac-

tion creates a phase difference between SST and rainfall anomalies. Figure 2 shows clear evidence that the organized rainfall anomalies tend to move northeastward toward areas of ocean-surface warming. The sea-surface warming caused by subdued convection in the dry phase of QMO may play an important role in steering the QMO convective anomalies toward an anomalously warm ocean surface. First, sea-surface warming may enhance energy flux into the atmosphere, which helps to destabilize the atmospheric boundary layer and build up convective available potential energy for organized deep convection (Stephens et al. 2004). Second, the surface-warming-induced sensible heat flux would lower surface pressure. This assertion is supported by the composite life cycle of rainfall anomalies and surface pressure anomalies, shown in Fig. 8. A pressure decrease tends to lead the enhanced rainfall by about one phase in the Bay of Bengal, where the northward propagation component is prominent. The positive SST-anomaly-induced lower surface pressure would, in turn, reinforce the boundary-layer convergence and promote organized deep convection to the northeast of the convection anomalies.

Another potentially important contributor is the vertical easterly shear in the monsoon region. How can the easterly vertical shear of the summer mean circulation contribute to northeastward propagation of the rainband? Wang and Xie (1997) demonstrated that the slanted rainband forms as a result of the continuing emanation of moist Rossby waves from the equatorial convective anomaly (an equatorial Kelvin–Rossby wave packet). Thus, the rainband has an eastward

**Fig. 8** Composite life cycle of sea-level pressure and rainfall anomalies (TRMM/TMI) in the Bay of Bengal (10–20°N, 85–95°E). The *bar* segments represent 90% confidence interval based on the Student *t*-test



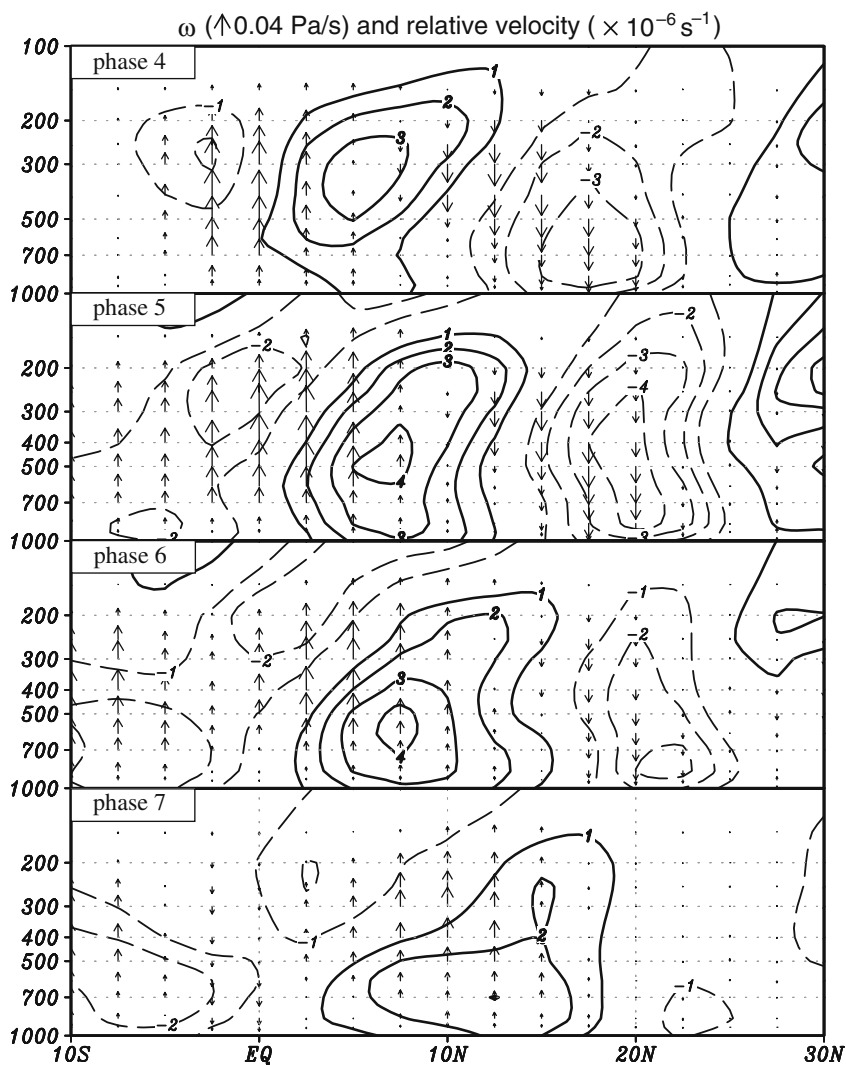
component following its equatorial eastward propagation. The individual moist Rossby wave moves westward; its northward component may be understood in terms of the effects of the mean flow on the moist Rossby waves. The cells embedded in the northwest/southeast-tilted rainband are convectively interactive Rossby waves (Wang and Xie 1997). A peculiar feature is that the relative vorticity anomalies associated with the QMO rainband have a barotropic structure, and the positive vorticity anomaly is located north of the corresponding anomalous convection center (Jiang et al. 2004). The positive vorticity, in turn, induces boundary-layer convergence, which destabilizes the atmosphere and triggers new convection to the north of the anomalous convection, thus favoring northward propagation. The result of Jiang et al. (2004) is derived for convection anomalies located at 5°N. To see whether or not this is a general case in all phases of northward propagation, we show the meridional vertical profiles of vertical motion and relative-vorticity anomalies along 90°E (Fig. 9). When the maximum upward motion is located around 5°N (Phases 5 and 6), the positive relative-vorticity anomaly below about 150 hPa is located about 3°–5° latitude to the north of the upward motion, which agrees with Jiang et al. (2004). However, the spatial phase difference between positive vorticity and upward motion decreases during the northward movement of the ISO rainband. Note also that the relative vorticity anomalies have a dominant barotropic structure but with a slightly northward tilt.

A key question is, how is the relative vorticity anomaly generated? Obviously, the barotropic vorticity anomalies cannot be directly forced by the convection, and there must be other reasons for its existence. Wang (2005) illustrated how a mean zonal flow with easterly vertical shear can generate such a barotropic vorticity anomaly. The interaction between barotropic mode and baroclinic mode in the presence of basic flow easterly vertical shear can be understood in terms of a two-layer equatorial beta plane model. To illustrate this mechanism, let us consider a simplified 2-D version of the model of Wang and Xie (1997) in which the zonal variations of the basic state and dependent variables are neglected. The vorticity equations for the barotropic component (denoted by the subscript ‘+’) is (refer to Wang and Xie for derivation) :

$$\frac{\partial \zeta_+}{\partial t} = -\beta v_+ - U_T \left( \frac{\partial \omega}{\partial y} \right), \tag{1}$$

where  $U_T$  denotes a constant vertical shear of the basic monsoon zonal flow. Equation 1 indicates that in the presence of vertical easterly shear ( $U_T < 0$  in  $p$ -coordinate), a northward decrease in the perturbation upward motion can generate positive barotropic vorticity to the north of the convection. Conversely, in the equatorward side it would produce negative barotropic vorticity. That explains how the vertical monsoon easterly shear interacting with moist Rossby waves can generate positive (negative)

**Fig. 9** Composite vertical structure of the QMO along 90°E (averaged between 85 and 95°E) from Phases 4 to 7. Shown are anomalies in vertical pressure velocity (arrows) and relative vorticity (contours in units of  $10^{-6} \text{ s}^{-1}$ ). The data used here were derived from ECMWF reanalysis



barotropic vorticity to the poleward (equatorward) side of the convective anomalies. Physically, the easterly vertical shear of the monsoon mean flow has a strong equatorward horizontal relative vorticity to the order of  $3 \times 10^{-2} \text{ ms}^{-1} \text{ hPa}^{-1}$ . The Rossby-wave-induced heating generates a perturbation vertical-motion field that decreases northward from the anomalous rain band center. This vertical-motion field twists the horizontal vorticity of the mean flow, generating a positive vertical component of relative vorticity to the north of the rainfall anomalies. For the same reason, negative vorticity anomalies develop to the south of the convection region. Thus, the interaction between moist Rossby-wave-induced heating and the vertical shear of the mean monsoon creates a condition that favors the northward movement of the enhanced rainfall.

## 8 Concluding remarks

With a suite of TRMM satellite measurements from 1998 to 2004, we examined the full cycle of the boreal summer ISO by compositing 28 individual events. Our major findings are summarized as follows.

- The average oscillation period during boreal summer over the Indian Ocean sector is about 32 days (Fig. 1). This quasi-monthly oscillation (QMO) is originated and reaches maximum strength in the EIO. The tropics-wide QMO is primarily confined to the tropical Indian and Pacific Oceans.
- The life cycles of wet QMO anomalies consist of four stages (Figs. 2, 3): (1) the initiation in the EIO between 60 and 70°E and subsequent development and eastward propagation along the

- equator; (2) the formation of a slanted band of rainfall anomalies tilted from the maritime continent to India; (3) the *northeastward* migration of the rain band in the northern Indian and western North Pacific Oceans, and (4) the rapid spread of these rainfall anomalies along the ITCZ to the ENP and concurrent slow northward migration to the Philippine Sea.
- (c) A marked east-west seesaw in the rainfall anomalies exist between the southern Bay of Bengal and the ENP (Fig. 5). In general, the anomalous ISO convection in the southern Bay of Bengal leads convection in the ENP by about 16 days. One may take advantage of this intraseasonal teleconnection to enhance predictability of the ISO in the ENP.
  - (d) During the initiation of the convective anomalies, the stratiform and convective rains have comparable rates; the prevailing cloud type experiences a *trimodal evolution* from shallow to deep convection, and finally to anvil and extended stratiform clouds (Fig. 6).
  - (e) SST-precipitation relation is found different between the equatorial and off-equatorial regions (Fig. 4). In the equatorial region, the simultaneous correlation between SST and rainfall anomalies is nearly zero; but in the off-equatorial region, significant negative correlation is found.

The observed evidence presented here provides critical information for validating the numerical models. The finding that the stratiform precipitation rate in the genesis region has the same order of magnitude as the convective precipitation may have important implications for numerical modeling of the ISO. The AGCMs that fail to simulate or that poorly simulate the ISO might have underestimated the portion of condensational heating released by stable precipitation.

The observed simultaneous negative correlation and the “asymmetric” SST-rainfall correlation in the off-equatorial region have important implications in monsoon climate simulation and prediction. As found by Wang et al. (2004) in a performance assessment of 11 atmospheric GCMs (AGCMs) that simulate summer monsoon precipitation, all models produce a positive simultaneous SST-rainfall correlation over the Philippine Sea and South China Sea, which is at odds with observations. The observations showed a negative simultaneous SST-precipitation correlation in these heavy precipitating summer monsoon regions when monthly anomalies are considered. The results here suggest that a negative SST-precipitation correlation

seen on monthly mean time scale may result from the *asymmetric* SST-rainfall relationship on the intraseasonal time scale. Over the off equatorial region, it is seen from Fig. 4 that the simultaneous correlation is negative, and the negative lag-correlation is stronger than the positive lead-correlation. The corresponding monthly mean SST-precipitation correlation is indeed negative (figure not shown).

Previous studies have termed summer monsoon oscillation during boreal summer as 30–60 day oscillation, suggesting that the boreal summer ISO has the same time scale as that of boreal winter MJO—the equatorial trapped mode. Based on most reliable TRMM precipitation estimation, we found the dominant periodicity over the Indian Ocean as is about 32 days rather than centered on 45 days (Fig. 1). This periodicity is determined from analysis of individual events which do not include the entire period of the boreal summer. Thus, discrepancies are expected between the current analysis and the previous spectral analysis. Our additional spectral analysis shows that the major spectral peak over the eastern EIO is at 30 days and in the ISM regions are in the range of 25–45 days, which supports the conclusion derived from Fig. 1. However, over the western Pacific, the peak is shifted to lower frequency around 45 days (figure not shown), which is in a better agreement with Chen and Murakami (1988). The QMO lifecycle patterns shown in Figs. 2 and 3, indeed consists of the previously reported “30–60 day” (may be more precisely 30–40 day) monsoon trough/ridge extending from India to the western Pacific (Krishnamurti and Subrahmanyam 1982; Lau and Chan 1986), as well as the trough-ridge system over the South China Sea (Chen and Murakami 1988). The movement of the precipitation anomalies suggests that the intraseasonal modes identified in the previous studies are interconnected as a whole system.

The 7-year summer data are not long, but it allows for selection of 28 events for the composite study, which gives a reasonable sampling for deriving mean behavior of QMO. The results derived from the 7-year data, however, need to be cautious because the data are not long enough to reflect possible decadal variations in QMO.

The theoretical analysis in Sect. 7 suggests that atmosphere-ocean interaction and the vertical monsoon easterly shear are important contributors to the northeastward propagation of the intraseasonal rain band. We should also note that the strong monsoon easterly vertical shear is a result of the land-ocean thermal contrast and the effects of the Tibetan plateau. In this sense, the land processes play an indirect but not

negligible role in sustaining northward propagation. The observed evidence presented here supports the self-induction mechanism theory for maintenance of the boreal summer ISO (WWT05).

Although this study offers explanations on aspects of the QMO, it leaves a number of issues unaddressed. Further clarification is needed about what determines the speed of the northward propagation component and the quasi-monthly time scale. Another issue is why the formation of the slanted rainband has preferred a location near Sumatra. It has been speculated that the decay of ISO over the maritime continent might involve multiple factors. For instance, the topographic blocking of the Sumatra Island (a mountain range higher than 2 km) could be destructive to the boundary layer organization of the MJO convection (Wang and Li 1994). The strong diurnal cycle over the Indonesian region is also an unfavorable condition because it constantly releases convective energy and might demolish the energy accumulation needed for development of convection on the intraseasonal time scale. Another possibility is the destructive land effects on air–sea interaction that is a positive contributor to the QMO. These possibilities deserve further investigation with numerical models.

**Acknowledgements** The authors thank Dr. R. Madden for his comments on an earlier version of the manuscript. Dr. Bin Wang acknowledges the support from NSF climate dynamics program (ATM03-29531) and in part by IPRC, which is in part sponsored by FRCGC.

## References

- Annamalai H, Slingo JM (2001) Active/break cycles: diagnosis of the intraseasonal variability of the Asian summer monsoon. *Clim Dyn* 18:85–102
- Chelton DB, Esbensen SK, Schlax G, Thum N, Freilich MH, Wentz FJ, Gentemann CL, McPhaden MJ, Schopf PS (2001) Observations of coupling between surface wind stress and sea surface temperature in the eastern tropical Pacific. *J Clim* 14:1479–1498
- Chen TC, Murakami M (1988) The 30–50 day variation of convective activity over the western Pacific–Ocean with emphasis on the northwestern region. *Mon Weather Rev* 116:892–906
- Duchon CE (1979) Lanczos filtering in one and two dimensions. *J Appl Meteorol* 18:1016–1022
- Fassulo J, Webster PJ (2000) Atmospheric and surface variations during westerly wind bursts in the tropical western Pacific. *Q J R Meteorol Soc* 126:899–924
- Ferranti L, Slingo JM, Palmer TN, Hoskins BJ (1997) Relations between interannual and intraseasonal monsoon variability as diagnosed from AMIP integrations. *Q J R Meteorol Soc* 123:1323–1357
- Fu X, Wang B (2004) Differences of boreal summer intraseasonal oscillations simulated in an atmosphere–ocean coupled model and an atmosphere-only model. *J Clim* 17:1263–1271
- Fu X, Wang B, Li T, McCreary JP (2003) Coupling between northward-propagating, intraseasonal oscillations and sea surface temperature in the Indian Ocean. *J Atmos Sci* 60:1733–1753
- Goswami BN, Shukla J (1984) Quasi-periodic oscillations in a symmetric general circulation model. *J Atmos Sci* 41:20–37
- Hartmann DL, Michelsen ML, Klein SA (1992) Seasonal variations of tropical intraseasonal oscillations: a 20–25-day oscillation in the western Pacific. *J Atmos Sci* 49:1277–1289
- Houze RA Jr (1993) *Cloud dynamics*. Academic, New York, pp 573
- Hsu HH, Weng CH (2001) Northwestward propagation of the intraseasonal oscillation in the western North Pacific during the boreal summer: structure and mechanism. *J Clim* 14:3834–3850
- Jiang XN, Li T (2005) Reinitiation of the boreal summer intraseasonal oscillation in the tropical Indian Ocean. *J Clim* (in press)
- Jiang XN, Li T, Wang B (2004) Structures and mechanisms of the northward propagating boreal summer intraseasonal oscillation. *J Clim* 17:1022–1039
- Johnson RH, Rickenbach TM, Rutledge SA, Ciesielski PE, Schubert WH (1999) Trimodal characteristics of tropical convection. *J Clim* 12:2397–2418
- Kemball-Cook S, Wang B (2001) Equatorial waves and air–sea interaction in the boreal summer intraseasonal oscillation. *J Clim* 14:2923–2942
- Kemball-Cook S, Weare BC (2001) The onset of convection in the Madden-Julian Oscillation. *J Clim* 14:780–793
- Kikuchi K, Takayabu YN (2004) The development of organized convection associated with the MJO during TOGA COARE: trimodal characteristics. *Geophys Res Lett* 31:L10101. DOI 10.1029/2004GL019601
- Krishnamurti TN, Subrahmanyam D (1982) 30–50-day mode at 850 mb during MONEX. *J Atmos Sci* 39:2088–2095
- Krishnan R, Zhang C, Sugi M (2000) Dynamics of breaks in the Indian summer monsoon. *J Atmos Sci* 57:1354–1372
- Kummerow C, Barnes W, Kozu T, Shiue J, Simpson J (1998) The Tropical Rainfall Measuring Mission (TRMM) sensor package. *J Atmos Ocean Technol* 15:809–817
- Kummerow C, Simpson J, Thiele O, Barnes W, Chang ATC, Stocker E, Adler RF, Hou A, Kakar R, Wentz F, Ashcroft P, Kozu T, Hong Y, Okamoto K, Iguchi T, Kuroiwa H, Im E, Haddad Z, Huffman G, Ferrier B, Olson WS, Zipser E, Smith EA, Wilheit TT, North G, Krishnamurti T, Nakamura K (2000) The status of the Tropical Rainfall Measuring Mission (TRMM) after two years in orbit. *J Appl Meteorol* 39:1965–1982
- Lau KM, Chan PH (1986) Aspects of the 40–50 day oscillation during the northern summer as inferred from outgoing longwave radiation. *Mon Weather Rev* 114:1354–1367
- Lau KM, Chan PH (1988) Intraseasonal and interannual variations of tropical convection: a possible link between the 40–50 day oscillation and ENSO? *J Atmos Sci* 45:506–521
- Lawrence DM, Webster PJ (2002) The boreal summer intraseasonal oscillation: relationship between northward and eastward movement of convection. *J Atmos Sci* 59:1593–1606
- Liu GS, Fu YF (2001) The characteristics of tropical precipitation profiles as inferred from satellite radar measurements. *J Meteorol Soc Jpn* 79:131–143
- Madden RA, Julian PR (1971) Detection of a 40–50 day oscillation in the zonal wind in the tropical Pacific. *J Atmos Sci* 28:702–708

- Madden RA, Julian PR (1972) Description of global scale circulation cells in the tropics with a 40–50 day period. *J Atmos Sci* 29:1109–1123
- Murakami T (1980) Temporal variations of satellite-observed outgoing longwave radiation over the winter monsoon region. Part I: Long-period (15–30 day) oscillations. *Mon Weather Rev* 108:408–426
- Murakami T, Wang B, Lyons SW (1992) Contrasts between Summer Monsoons over the Bay of Bengal and the Eastern North Pacific. *J Meteorol Soc Jpn* 70:191–210
- National Aeronautics and Space Administration (2001) QuikSCAT science data product user's manual, overview and geophysical data product, version 2.2. Jet Propulsion Laboratory, California Institute of Technology, Pasadena, CA, 89 p. (Available at [http://www.podaac.jpl.nasa.gov/quikscat/qscat\\_doc.html](http://www.podaac.jpl.nasa.gov/quikscat/qscat_doc.html))
- Rodwell MJ (1997) Breaks in the Asian monsoon: the influence of Southern Hemisphere weather systems. *J Atmos Sci* 54:2597–2611
- Salby ML, Hendon HH (1994) Intraseasonal behavior of clouds, temperature, and motion in the tropics. *J Atmos Sci* 51:2207–2224
- Sikka DR, Gadgil S (1980) On the maximum cloud zone and the ITCZ over Indian longitudes during the southwest monsoon. *Mon Weather Rev* 108:1840–1853
- Slingo J, Inness P, Neale R, Woolnough S, Yang GY (2003) Scale interactions on diurnal to seasonal timescales and their relevance to model systematic errors. *Ann Geophys* 46:139–155
- Stephens GL, Webster PJ, Johnson RH, Engelen R, L'Ecuyer T (2004) Observational evidence for mutual regulation of the tropical hydrological cycle and tropical sea surface temperature. *J Clim* 17:2213–2224
- Vecchi G, Harrison DE (2002) Monsoon breaks and sub-seasonal sea surface temperature variability in the Bay of Bengal. *J Clim* 15:1485–1493
- Waliser DE, Lau KM, Kim JH (1999) The influence of coupled sea surface temperatures on the Madden-Julian oscillation: a model perturbation experiment. *J Atmos Sci* 56:333–358
- Waliser DE, Jin K, Kang IS, Stern WF, Schubert SD, Wu MLC, Lau KM, Lee MI, Krishnamurthy V, Kitoh A, Meehl GA, Galin VY, Satyan V, Mandke SK, Wu G, Liu Y, Park CK (2003) AGCM simulations of intraseasonal variability associated with the Asian summer monsoon. *Clim Dyn* 21:423–446
- Wang B (2005) Theory in Intraseasonal variability in the Atmosphere-Ocean climate system. Praxis Books, Praxis Publishing Ltd, Chichester, UK, p 474
- Wang B, Rui H (1990) Synoptic climatology of transient tropical intraseasonal convection anomalies: 1975–1985. *Meteorol Atmos Phys* 44:43–61
- Wang B, Li T (1994) Convective interaction with boundary-layer dynamics in the development of a tropical intraseasonal system. *J Atmos Sci* 51:1386–1400
- Wang B, Xie X (1997) A model for the boreal summer intraseasonal oscillation. *J Atmos Sci* 54:72–86
- Wang B, Kang IS, Lee JY (2004) Ensemble simulations of Asian–Australian monsoon variability by 11 AGCMs. *J Clim* 17:803–818
- Wang B, Webster PJ, Teng H (2005) Antecedents and self-induction of active-break Indian monsoon unraveled by satellites. *Geophys Res Lett* 32:L04704. DOI 10.1029/2004GL020996
- Webster PJ (1983) Mechanisms of monsoon low-frequency variability: surface hydrological effects. *J Atmos Sci* 40:2110–2124
- Webster PJ, Magana VO, Palmer TN, Shukla J, Tomas RA, Yanai M, Yasunari T (1998) Monsoon: processes, predictability, and the prospects for prediction. *J Geophys Res* 103:14451–14510
- Webster PJ, Bradley EF, Fairall CW, Godfrey JS, Hacker P, Houze RA Jr, Lukas R, Serra Y, Hummon JM, Lawrence TDM, Russel CA, Ryan MN, Sahami K, Zuidema P (2002) The joint air–sea monsoon interaction experiment (JASMIN) pilot study. *Bull Am Meteorol Soc* 83:1603–1630
- Wentz FJ, Spencer RW (1998) SST/I rain retrievals within a unified all-weather ocean algorithm. *J Atmos Sci* 55:1613–1627
- Wheeler MC, Hendon HH (2004) An all-season real-time multivariate MJO index: development of an index for monitoring and prediction. *Mon Weather Rev* 132:1917–1932
- Wu MLC, Schubert S, Kang IS, Waliser DE (2002) Forced and free intra- seasonal variability over the south Asian monsoon region simulated by 10 AGCMs. *J Clim* 15:2862–2880
- Wu Z (2003) A shallow CISK, deep equilibrium mechanism for the interaction between large scale convection and large scale circulations in the tropics. *J Atmos Sci* 60:377–392
- Yasunari T (1979) Cloudiness fluctuations associated with the Northern hemisphere summer monsoon. *J Meteorol Soc Jpn* 57:227–242
- Yasunari T (1980) A quasi-stationary appearance of 30 to 40 day period in the cloudiness fluctuations during the summer monsoon over India. *J Meteorol Soc Jpn* 58:225–229